TABLE 1
Results of Assessment of Digital Overlay in 22 Wrists by Three Observers

Observer	Abnormal without digital overlay	Abnormal with digital overlay	Improved localization
1	19	22	3
2	16	22	6
3	10	22	12

DISCUSSION

The evaluation of wrist pain, after trauma, is a common clinical problem. The sensitivity of bone scintigram is approximately 100%, and the specificity is found to be maximally 98% [95% C.I. 88%–100%], but sometimes it is difficult to give an exact localization of the hot spot seen on the bone scan, especially of the carpus. This was found in our academic institution with a specific interest in the diagnostic imaging of scaphoid fractures.The specificity is probably less in a general nuclear medicine department lacking special expertise in this area.

CONCLUSION

In this study the digital overlay technique clearly improved the interpretation of the localization of the carpal hot spot, which may lead to a higher specificity of the bone scan. The hand-fix proved to be a simple acrylic device for matching the images. A multimodality program must be available for producing these overlaid images. Our results demonstrate that this application significantly improves the diagnostic effectiveness of routine bone scan imaging in hand and wrist injuries. However, the hand-fix device used in this study could be improved. The height of the marker cylinders induced a small parallax error (seen in Fig. 2 A, B). This error can be reduced if the heights of the marker cylinders are reduced.

This technique, in which a videocamera was used to digitize the radiographs, can be further simplified if the acquisition of scaphoid series is also digital. In that case, a network connection between the radiology and nuclear medicine departments is required. Otherwise, a good quality film digitizer or videocamera and frame grabber board can be used.

ACKNOWLEDGMENTS

We thank the nuclear medicine physician and the two residents for judging the bone scans and the technologists of the radiology department for their help.

REFERENCES

1. Tiel-van Buul MMC, van Beek EJR, Broekhuizen AH, Nooitgedacht EA, Davids PHP, Bakker AJ. Diagnosing scaphoid fractures: radiographs cannot be used as a gold standard. *Injury* 1992;23:77–79.
2. Shewring DJ, Savage R, Thomas G. Experience of the early use of technetium-99 bone scintigraphy in wrist injury. *J Hand Surg [Br]* 1994;19B:114–117.
3. Waizenegger M, Wastie ML, Barton NJ, Davis RC. Scintigraphy in the evaluation of the "clinical"scaphoid fracture. *Hand Surg [Br]* 1994;19B:6: 750–753.
4. Tiel-van Buul MMC, van Beek EJR, Dijkstra PF, Bakker AJ, Broekhuizen AH, van Royen EA. Significance of a hot spot on the bone scan after carpal injury–evaluation by computed tomography. *Eur J Nucl Med* 1993;20:159–164.
5. Alpert NM, Bradshaw JF, Kennedy D, Correia JA. The principal axes information–a method for image registration. *J Nucl Med* 1990;31:1717–1722.
6. Lehmann ED, Hawkes DJ, Hill DLG, Bird CF, Robinson GP, Colchester ACF, Maisey MN. Computer-aided interpretation of SPECT images of the brain using an MRI-derived three-dimensional neuro-anatomical atlas. *Med Inform* 1991;16:151–166.
7. Slomka PJ, Hurwitz GA, Stephenson J, Cradduck T. Automated alignment and sizing of myocardial stress and rest scans to three-dimensional normal templates using an image registration alogrithm. *J Nucl Med* 1995;36:115–122.
8. Henze E, Graf G, Clausen M, et al. The orthopan tomoscintigram–a new application of emission computed tomography for facial bone scanning. *Eur J Nucl Med* 1990;16:97–101.
9. Slomka PJ, Hurwitz GA, Stepehenson JA, et al. A volume-based image registration toolkit for automated comparison of paired nuclear medicine images [Abstract]. *Med Phys* 1995:22:1017.

Internal Dose Estimation Including the Nasal Cavity and Major Airway for Continuous Inhalation of $C^{15}O_2$, $^{15}O_2$ and $C^{15}O$ Using the Thermoluminescent Dosimeter Method

H.M. Deloar, H. Watabe, T. Nakamura, Y. Narita, A. Yamadera, T. Fujiwara and M. Itoh
Cyclotron and Radioisotope Center, Tohoku University, Aoba, Aramaki, Japan

In the steady state method, ^{15}O-labeled gases ($C^{15}O_2$, $^{15}O_2$ and $C^{15}O$) are administered to the body by continuous inhalation in various clinical PET studies. During inhalation, the nasal cavity and major airway may obtain a substantial amount of dose, being the source organs as well as the target organs. The internal absorbed dose to those organs and their contribution to the other target organs have not been calculated by the MIRD method. To calculate the internal dose in the MIRD method, the S values, the absorbed doses per unit of cumulated activities from nasal cavity and major airway to the other organs and vice versa, are needed, and these values are not available. **Methods:** In this study, we introduced a mathematical model of the nasal cavity and major airway to calculate their S values to 23 target organs and from 11 source organs to them. Individual experiments were performed to measure the total uptake percentage and body surface doses of ^{15}O-labeled gases from continuous inhalation. **Results:** Using the body surface doses measured by thermoluminescent dosimeters, the cumulated activities of 11 source organs were estimated with the mathematical transformation method, and then the internal absorbed doses in 23 target organs were calculated by the MIRD method. Our experimental results were compared with the other results, and good agreements were observed. **Conclusion:** Among the target organs, the critical organ is the airway, and the absorbed dose is 2.57×10^{-2} mGy · MBq^{-1}.

Key Words: steady state technique; TLD; MIRD method; ^{15}O inhalation; SAF

J Nucl Med 1997; 38:1603–1613

Received Jun. 3, 1996; accepted Nov. 6, 1996.

For correspondence or reprints contact: Prof. T. Nakamura, Cyclotron and Radioisotope Center, Tohoku University, Aoba, Aramaki, Aoba-ku, Sendai-980, Japan.

In the steady state technique (*1–3*), ^{15}O-labeled gases are routinely used in clinical PET studies because of the short half-life (2 min) of ^{15}O and limited radiation exposure. The gases of $C^{15}O_2$, $^{15}O_2$ and $C^{15}O$ are successively administered into the body through continuous inhalation for multiple clinical studies, such as the measurement of cerebral blood flow, cerebral blood volume and oxygen extraction fraction in the same subject.

Internal radiation absorbed doses in target organs were estimated (*4,5*) using the steady state technique, where the lung, for all three gases (*4*), and the spleen, for $C^{15}O$ (*5*), were considered to be the critical organs at highest risk. The nasal cavity and major airway were, however, not considered in the dose calculation procedure. Powell et al. (*6*) reported that the tracheal mucosal layer absorbed a considerable amount of dose during inhalation of $C^{15}O_2$, and the retention was around 30% after a single breath. Meyer et al. (*7*) found that the ratio of mean tracheal activity of $C^{15}O_2$ to $^{15}O_2$ is 5.3. Tracheal dose has been estimated by direct PET measurement on humans (*6,7*) and by thermoluminescent dosimeter (TLD) measurement on Lucite tracheal phantom (*8*). By the direct sampling and ^{15}O assaying of mucus and saliva from the linings of the airways in humans and dogs, the tracheal dose has also been calculated (*9*). Although the absorbed doses from these measurements are incompatible with each other, the results revealed that the airway, which includes pharynx, larynx and trachea, is the organ with the highest dose accumulation and that it must be considered a target organ as well as a source organ. In this study, we then calculated the absorbed doses of all target organs, including the nasal cavity and major airway with the MIRD method (*10*). To calculate the dose with the MIRD method, S values (absorbed dose per unit of cumulated activity) for all source organs to target organs are required. It is also necessary to know the cumulated activities of all source organs. We first calculated the S values of the nasal cavity and major airway by using a mathematical model based on the anatomical data of those organs incorporated into the MIRD phantom (*11*). The S values of all source organs to target organs, including nasal cavity and major airway, have been calculated with the VADMAP (SAF calculation) code (*12*).

In the MIRD method, estimation of activities cumulated in source organs is an essential but difficult task. During the PET study, our group has developed a new method (*13*) to obtain the organ biodistribution of cumulated activities of the source organs through the use of TLDs. Without impeding clinical studies, this method is suitable for calculating the cumulated activities of source organs for any kind of radiopharmaceuticals. In this TLD method, several TLDs are placed on the body surface, just above the source organs during the PET study. Because the dose obtained by the TLD should be equal to the source organ's cumulated activity times the S value of the source organ to a TLD, the cumulated activities of source organs can be calculated by applying a slightly modified SAND-II unfolding code (*14,15*), an inverse transformation method. In this study, we applied this TLD method to estimate the biodistribution of radioactivities in the source organs from continuous inhalation of gases.

To estimate the absorbed dose from the continuous inhalation, it is also necessary to know the uptake fraction of inhaled gas. Considering the biological distribution of metabolic process, the total uptakes of various ^{15}O-labeled gases were estimated by Bigler et al. (*4*). Kearfott (*5*) reported the complete uptake of the $C^{15}O$ bolus inhalation when the breath was held for 20 sec. It was assumed that the uptake and retention periods were equivalent during continuous inhalation. In this study we also performed an experiment to measure the percentage of uptake due to continuous inhalation of ^{15}O-labeled gases.

Finally, the absorbed doses in 23 target organs were estimated according to the MIRD method for continuous inhalation of three gases of $C^{15}O_2$, $^{15}O_2$ and $C^{15}O$.

MATERIALS AND METHODS

During clinical PET studies at the Cyclotron and Radioisotope Center (CYRIC), Tohoku University, two independent studies were performed to estimate radiation doses during successive continuous inhalation of ^{15}O-labeled gases ($C^{15}O_2$, $^{15}O_2$ and $C^{15}O_2$). One study measured the percentage uptake of inhaled gases; the other estimated the body surface doses with TLDs. The uptake percentage measurements were done on 10 subjects, and body surface doses were measured on another 7 subjects. The ages of the subjects were 13–30 yr. The flow rates were 370–740 MBq/min for $C^{15}O_2$ and $^{15}O_2$ and 259–481 MBq/min for $C^{15}O$, and the rates were controlled by a radio gas controller. The subjects inhaled the gases sequentially (first, $C^{15}O_2$; second, $^{15}O_2$; third, $C^{15}O$) under their own control. The inhalation periods for $C^{15}O_2$ and $^{15}O_2$ were 10–15 min, and the period for $C^{15}O$ was 2–5 min. For the measurements of the body surface doses with TLDs, five subjects were adult and two were children (13 yr old). We then divided our internal dose estimation study into two groups: one for adults and the other for 13-yr-old children.

Mathematical Phantom and S Value Calculation of Nasal Cavity and Major Airway

In this study, we considered the nasal cavity and major airway as both source organs and target organs to calculate the corresponding S values from source organs to target organs, which are essential for the dose calculation procedure. Because those values are already available (*11,12,16*), except in the case of the nasal cavity and major airway, we calculated the S values of these two organs with the VADMAP code (*12*) based on the point-kernel method.

In this procedure, a point from which a photon is emitted is randomly selected in a source organ. The specific absorption fraction (SAF) for direct and scattered gamma rays can then be calculated according to the following equation:

$$\Phi(j \leftarrow i) = \frac{\mu_{en}}{\rho} \frac{1}{4\pi r^2} B(\mu r) e^{-\mu r}, \qquad \text{Eq. 1}$$

where $\Phi(j \leftarrow i)$ is the SAF from the i-th source organ to the j-th target organ at the distance r from the source; ρ is the density of the medium; μ and μ_{en} are the linear attenuation and energy absorption coefficients of that medium, respectively. In the MIRD phantom given by Cristy and Eckerman (*11*), the medium is water, which has a density of 1.468 g/cm^3 for skeleton tissue, 0.2958 g/cm^3 for lung tissue and 0.9869 g/cm^3 for remainder of the body. $B(\mu r)$ is the dose buildup factor, which represents the scattering component. It was calculated by Harima et al. (*17*) using an approximate analytical formula called the geometrical progression method. The S value of source i to target j can then be calculated as follows:

$$S(j \leftarrow i) = KnE\Phi(j \leftarrow i), \qquad \text{Eq. 2}$$

where K is a constant, n is the number of particles emitted per transition and E is the mean energy per particle. For positron emitters, n = 2 and E = 0.511 MeV.

To calculate the S value of the airway, a geometrical model is necessary. The shape of the airway is asymmetric, i.e., the nasal cavity in the upper part is like a hemisphere, and the rest is like an elliptical cylinder. For our convenience, we divided the airway into two parts: the nasal cavity including pharynx and the major airway, which

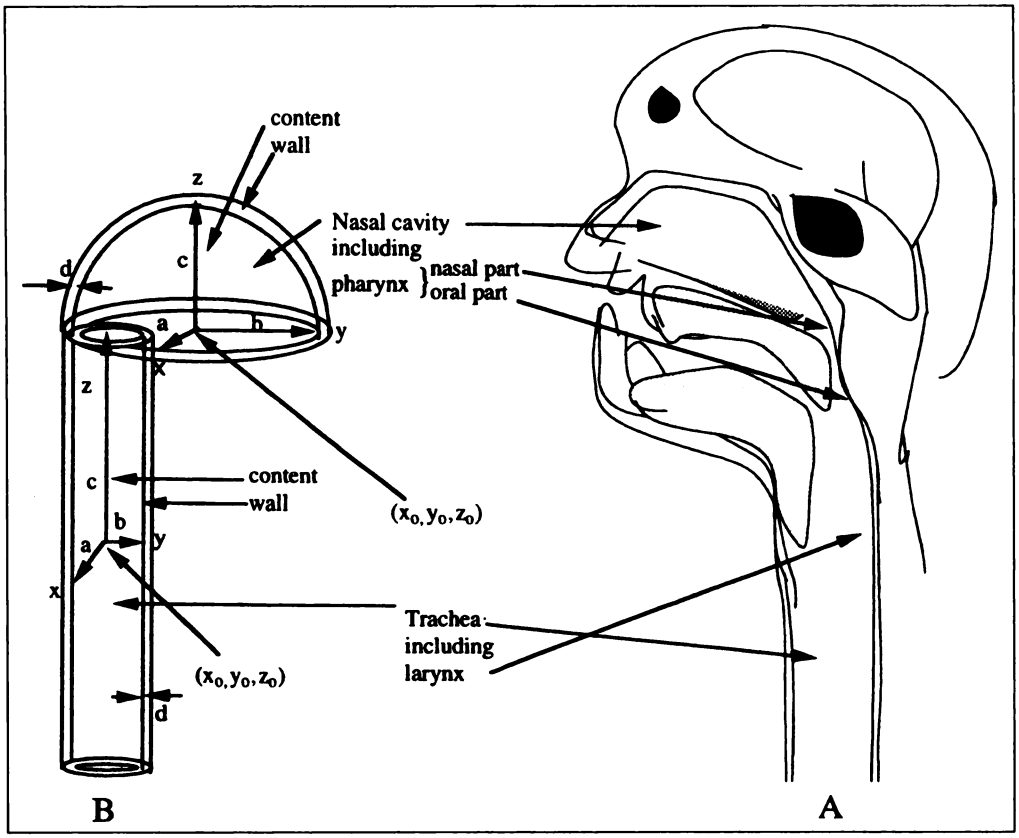

FIGURE 1. Schematic diagram of the nasal cavity and major airway (A) and the corresponding mathematical model (B) in Cartesian coordinates for calculation of S value. a, b and c are the radii of x, y and z axes, respectively, and d is the thickness of the wall.

defined the geometry of those organs by the following mathematical equations and introduced it in the VADMAP code.

Nasal cavity can be expressed by half of anellipsoid as follows. For nasal cavity content:

$$\left(\frac{x - x_o}{a - d}\right)^2 + \left(\frac{y - y_o}{b - d}\right)^2 + \left(\frac{z - z_o}{c - d}\right)^2 \leq 1, \quad \text{Eq. 3}$$

where $z_o \leq z \leq z_o + c - d$.

For nasal cavity wall:

$$\left(\frac{x - x_o}{a}\right)^2 + \left(\frac{y - y_o}{b}\right)^2 \leq 1 \quad \text{Eq. 4}$$

when $z_o - d \leq z \leq z_o$, and

$$\left(\frac{x - x_o}{a - d}\right)^2 + \left(\frac{y - y_o}{b - d}\right)^2 + \left(\frac{z - z_o}{c - d}\right)^2 \geq 1 \quad \text{Eq. 5}$$

and

$$\left(\frac{x - x_o}{a}\right)^2 + \left(\frac{y - y_o}{b}\right)^2 + \left(\frac{z - z_o}{c}\right)^2 \leq 1 \quad \text{Eq. 6}$$

when $z_o \leq z \leq z_o + c$. a, b and c are the radii along x, y and z axes, respectively. The central position of the organ in Cartesian coordinates is fixed at the floor of the cavity (x_o, y_o, z_o), and d is the thickness of the nasal cavity wall.

The major airway can be expressed by an elliptical cylinder as follows. For major airway content:

$$\left(\frac{x - x_o}{a - d}\right)^2 + \left(\frac{y - y_o}{b - d}\right)^2 \leq 1 \quad \text{Eq. 7}$$

when $z_o - c \leq z \leq z_o + c$.

For major airway wall:

$$\left(\frac{x - x_o}{a}\right)^2 + \left(\frac{y - y_o}{b}\right)^2 \leq 1 \quad \text{Eq. 8}$$

and

$$\left(\frac{x - x_o}{a - d}\right)^2 + \left(\frac{y - y_o}{b - d}\right)^2 \geq 1 \quad \text{Eq. 9}$$

when $z_o - c \leq z \leq z_o + c$. a, b and c are the radii along x, y and z axes, respectively. The central position of the organ in Cartesian coordinates is (x_o, y_o, z_o), and d is the thickness of the major airway wall.

The anatomical data of the nasal cavity and major airway are shown in Tables 1 and 2, respectively. The a, b, c and d values for adults were estimated by three-dimensional CT measurements (Takenori Hachiya, Research Institute for Brain and Blood Vessels,

TABLE 1
Phantom Data for Nasal Cavity

Age	a (cm)	b (cm)	c (cm)	d (cm)	x_o (cm)	y_o (cm)	z_o (cm)
Adult	1.38	4.3	5.7	0.3	0	4.74	80.6
15 yr	1.189	4.21	5.17	0.2745	0	4.626	72.64
13 yr	1.082	3.964	4.704	0.253	0	4.023	65.59
10 yr	0.975	3.717	4.238	0.2315	0	3.42	58.55

TABLE 2
Phantom Data for Major Airways

Age	a (cm)	b (cm)	c (cm)	d (cm)	x_o (cm)	y_o (cm)	z_o (cm)
Adult	0.77	1.38	11.47	0.3	0	1.82	69.07
15 yr	0.663	1.35	10.41	0.275	0	1.776	62.25
13 yr	0.604	1.225	9.469	0.253	0	1.656	56.21
10 yr	0.544	1.19	8.53	0.235	0	1.536	50.17

TABLE 3
SAF for 70-kg Adult Using 0.51-MeV Energy

Target organ	Source organ					
	Brain	Heart	Lung	Liver	Spleen	Kidney
Adrenal	2.039E-07	1.257E-05	1.144E-05	3.523E-05	9.821E-06	4.081E-05
Major airway (wall)	1.138E-05	7.876E-06	1.056E-05	1.228E-06	1.096E-06	7.301E-07
Nasal cavity (wall)	9.056E-05	7.958E-07	1.622E-06	2.132E-07	2.064E-07	1.459E-07
Bladder (wall)	8.557E-09	3.910E-07	3.470E-07	1.245E-06	1.080E-06	1.820E-06
Stomach (wall)	1.257E-07	1.050E-05	6.667E-06	7.716E-06	3.222E-05	1.274E-05
SI (wall)	3.358E-08	1.668E-06	1.453E-06	7.106E-06	5.572E-06	1.051E-05
ULI (wall)	3.624E-08	1.855E-06	1.646E-06	9.839E-06	5.534E-06	1.084E-05
LLI (wall)	1.355E-08	6.145E-07	5.908E-07	1.248E-06	2.921E-06	3.349E-06
Kidney	9.402E-08	4.543E-06	2.756E-06	1.479E-05	3.437E-05	4.480E-04
Liver	1.466E-07	1.081E-05	9.329E-06	7.439E-05	4.485E-06	1.362E-05
Lung	9.455E-07	2.023E-05	1.106E-04	8.692E-06	9.473E-06	2.391E-06
Ovary	1.686E-08	7.704E-07	5.904E-07	2.788E-06	2.501E-06	5.725E-06
Pancreas	1.614E-07	1.483E-05	9.143E-06	1.757E-05	5.681E-05	2.461E-05
Spleen	1.422E-07	7.247E-06	8.903E-06	4.357E-06	3.925E-04	3.021E-05
Testes	3.214E-09	1.316E-07	1.208E-07	4.012E-07	3.383E-07	5.592E-07
Thymus	1.168E-06	3.693E-05	1.468E-05	3.749E-06	2.344E-06	1.573E-06
Thyroid	9.092E-06	3.189E-06	5.375E-06	6.709E-07	5.646E-07	3.765E-07
Uterus	1.601E-08	7.136E-07	6.727E-07	2.598E-06	2.265E-06	4.091E-06
Breast	5.539E-07	1.551E-05	3.700E-06	4.878E-06	3.139E-06	2.181E-06
Brain	1.633E-04	5.621E-07	1.166E-06	1.524E-07	1.418E-07	9.223E-08
Heart	5.118E-07	1.832E-04	2.108E-05	1.161E-05	8.487E-06	4.785E-06
Red marrow	3.633E-06	5.207E-06	6.847E-06	4.890E-06	5.464E-06	9.131E-06
Bone, surface	4.887E-06	3.582E-06	4.953E-06	2.401E-06	3.125E-06	4.308E-06

SI = small intestine; ULI = upper large intestine; LLI = lower large intestine.

Akita, Japan, *personal communication*, 1995) and then introduced to the MIRD phantom (*11*). The central positions of the nasal cavity and major airway, x_o, y_o and z_o, in Tables 1 and 2, were determined very carefully to incorporate them into the MIRD phantom. The data of nasal cavity and major airway, except in the case of the adults, were estiated from the MIRD phantom, considering the age dependency of organ sizes of gastrointestinal tract, upper large intestine, lower large intestine and urinary bladder, because those organs have the wall and content similar to these two organs. The various geometrical parameters of the nasal cavity and major airway for children of age t were calculated from the following logarithmic mean:

$$R_v(t) = \left\{ \prod_{i=1}^{4} \frac{P_i(t)}{P_i(\text{adult})} \right\}^{1/4} \times R_v(\text{adult}), \qquad \text{Eq. 10}$$

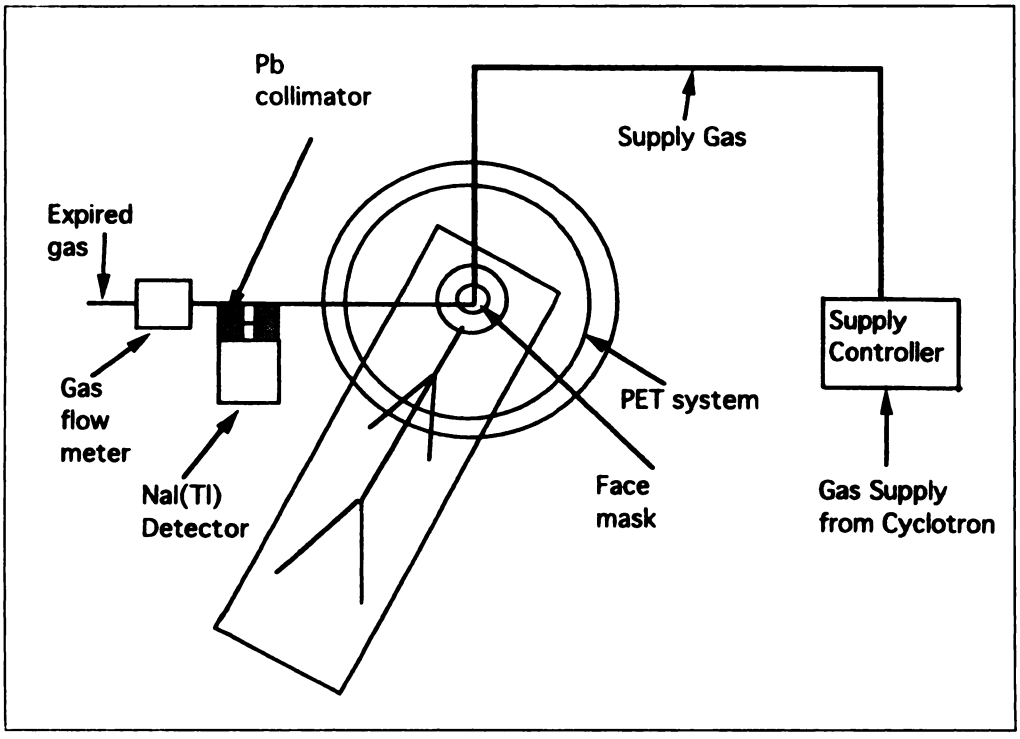

FIGURE 2. Schematic view of the uptake measurement of ^{15}O-labeled gases due to continuous inhalation.

TABLE 4
SAF for 70-kg Adult Using 0.51-MeV Energy

Target organ	Source organ				
	Pancreas	Bladder	Total body	Nasal cavity	Major airway
Adrenal	3.294E-05	8.774E-07	4.321E-06	3.124E-07	1.957E-06
Major airway (wall)	1.411E-06	5.963E-08	5.706E-06	4.883E-05	4.215E-04
Nasal cavity (wall)	2.353E-07	1.235E-08	4.485E-06	5.735E-04	2.964E-05
Bladder (wall)	1.281E-06	2.584E-04	4.769E-06	1.265E-08	6.434E-08
Stomach (wall)	5.951E-05	1.692E-06	5.944E-06	1.754E-07	9.769E-07
SI (wall)	7.202E-06	1.095E-05	6.500E-06	4.749E-08	2.358E-07
ULI (wall)	9.004E-06	7.961E-06	7.107E-06	5.404E-08	2.816E-07
LLI (wall)	2.493E-06	2.609E-05	6.004E-06	1.912E-08	9.709E-08
Kidney	2.349E-05	1.820E-06	6.184E-06	1.494E-07	7.860E-07
Liver	1.703E-05	1.305E-06	5.142E-06	2.922E-07	1.175E-06
Lung	8.478E-06	2.599E-07	7.703E-06	1.383E-06	1.027E-05
Ovary	2.745E-06	2.374E-05	6.325E-06	2.507E-08	1.144E-07
Pancreas	5.891E-04	1.274E-06	6.347E-06	2.420E-07	1.368E-06
Spleen	7.182E-05	1.074E-06	5.634E-06	2.101E-07	1.064E-06
Testes	3.863E-07	1.980E-05	6.241E-06	4.496E-09	2.094E-08
Thymus	3.653E-06	1.664E-07	5.993E-06	1.576E-06	1.262E-05
Thyroid	7.025E-07	3.688E-08	5.411E-06	1.095E-05	2.976E-05
Uterus	2.722E-06	5.421E-05	5.391E-08	2.327E-08	1.157E-07
Breast	4.385E-06	2.456E-07	3.364E-06	6.927E-07	3.430E-06
Brain	1.590E-07	8.652E-09	1.327E-05	1.263E-07	1.089E-05
Heart	1.604E-05	4.014E-07	5.633E-06	7.570E-07	6.175E-06
Red marrow	7.234E-06	4.582E-06	5.105E-06	7.674E-06	1.061E-05
Bone, surface	3.394E-06	1.840E-06	4.144E-06	8.204E-06	8.381E-06

SI = small intestine; ULI = upper large intestine; LLI = lower large intestine.

where i = 1–4 represents the gastrointestinal tract, upper large intestine, lower large intestine and urinary bladder; $R_v(t)$ and $R_v(\text{adult})$ are any geometrical parameter (a, b, c, d, etc.) of nasal cavity or major airway. $P_i(t)$ and $P_i(\text{adult})$ are any geometrical parameter (a, b, c, d, etc.) of gastrointestinal tract, upper large intestine, lower large intestine and urinary bladder, which are already known from the MIRD phantom (*11*). Because phantom data of all organs for 13 yr are not available, we interpolated those data from the MIRD (*11*) phantom for 10 and 15 yr.

We have calculated the SAF values of various ages for 11 source organs (brain, nasal cavity, upper respiratory tract, heart, lung, liver, spleen, kidney, pancreas, bladder and remainder of the body) to 23 target organs. The remainder of the body was assumed to be a single source organ. In Tables 3 and 4, we only show the SAF values of adults for 0.511-MeV photon energy.

Basic Theory

In the MIRD method (*10*), the internal absorbed dose from source to target organs is given as follows:

$$D_i = \sum_j S(i \leftarrow j)\tilde{A}_j = \sum_j S_{i,j}\tilde{A}_j, \quad \text{Eq. 11}$$

where D_i is the absorbed dose in the i-th target organ, $S_{i,j}$ is the absorbed dose in the i-th target organ per unit of cumulated activity of the j-th source organ and $\tilde{A}_j$ is the cumulated activity of the j-th source organ.

In our TLD method, several TLDs are placed on the body surface near the source organs, and the body surface doses are measured by TLDs. The body surface dose measured by the TLDs can be expressed as:

$$T_i = \sum_j R_{i,j}X_j, \quad \text{Eq. 12}$$

where T_i is the body surface dose measured at the i-th TLD position, $R_{i,j}$ is the absorbed dose at the i-th TLD position per unit of cumulated activity of the j-th source organ, and X_j is the cumulated activity of the j-th source organ integrated during the TLD attachment.

The T-vector is known from the TLD measurements, and the R-matrix can be calculated by the MIRD phantom and the VADMAP code using Equations 1 and 2. Then, with an inverse transformation of Equation 12, the X-vector can be calculated.

Cumulated Activity of Total Uptake

In the inverse transformation of Equation 12 and in the internal absorbed dose calculation of Equation 11, the cumulated activity of total uptake of the individual gas must be determined. It can be expressed by:

$$\tilde{A} = f\left(\int_0^t \frac{A_o}{\lambda}(1 - e^{-\lambda\tau})\,d\tau + \int_t^\infty \frac{A_o}{\lambda}(1 - e^{-\lambda t})\,e^{-\lambda(\tau - t)}\,d\tau\right) = f\frac{A_o}{\lambda}t, \quad \text{Eq. 13}$$

where A_o is the flow rate of the gas in MBq · min^{-1}, λ is the decay constant for ^{15}O, t is the inhalation period in min and f is the uptake percentage of the individual gas. The first integration term of Equation 13 is the cumulated activity during the inhalation period, and the second term is the cumulated activity after inhalation stops, considering only physical decay of the activity.

Background Estimation and Subtraction

Among the TLD positions as described later, the positions (see positions 1–4 in Fig. 3) near the brain, nasal cavity, thyroid and

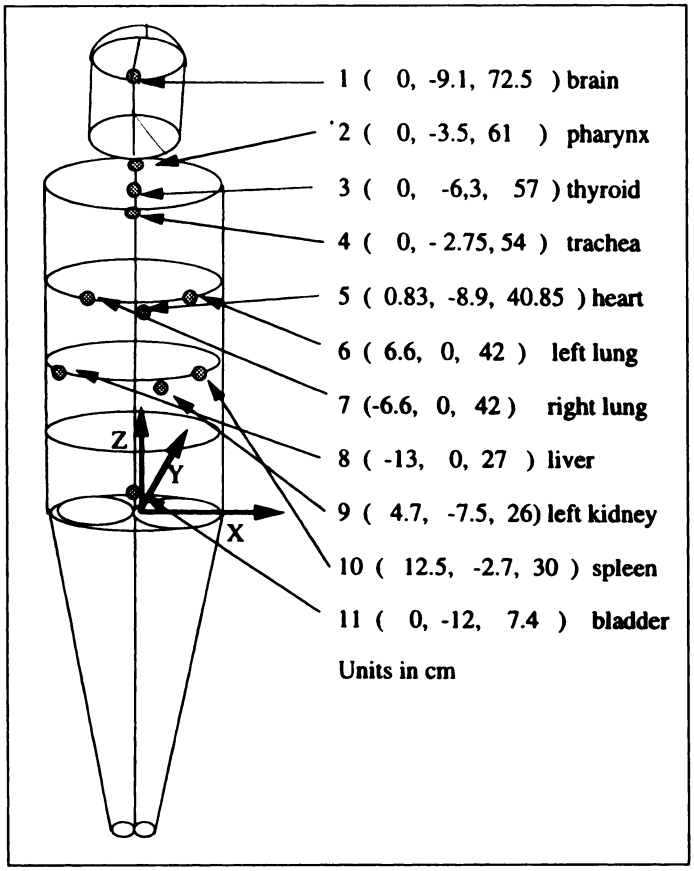

FIGURE 3. TLD positions with their Cartesian coordinates on a 13-yr-old's MIRD phantom for the body surface dose measurement.

upper respiratory tract are very close to the face gas mask (Fig. 2). These TLDs receive a remarkable amount of background radiation from the gas mask. Hence, the body surface doses obtained by these TLDs are the doses due to the internal radiation transmitted through the body from the source organs and the external background radiation from the gas mask, inlet and outlet pipes. The estimation and subtraction of external background radiation is important in obtaining the real body-surface dose due to the internal radiation. Practically, the background subtraction is very difficult, and we have done it by simulation. By considering three external background sources, the gas mask, inlet and outlet gas pipes, the external background dose may be defined as:

$$D_j(bg) = \tilde{A}_m S(j \leftarrow m) + \tilde{A}_i S(j \leftarrow i) + \tilde{A}_o S(j \leftarrow o), \quad \text{Eq. 14}$$

where j represents the j-th TLD position in Figure 3; m, i and o represent the respective background sources of the gas mask, inlet and outlet gas pipes, respectively, in Figure 2; S(j ← m), S(j ← i) and S(j ← o) are the S factors of the gas mask, inlet and outlet pipes, respectively, to all TLD positions; and $\tilde{A}_m$, $\tilde{A}_i$ and $\tilde{A}_o$ are the respective cumulated activities. The cumulated activities of the three sources were calculated from the following relation:

$$\tilde{A}_m = A_c t, \quad \text{Eq. 15}$$

where c represents m (mask), i (inlet pipe) or o (outlet pipe), and t is the inhalation period (residence time) of a single gas ($C^{15}O_2$, $^{15}O_2$ or $C^{15}O_2$). As the gases continuously flow through the inlet and outlet pipes, the flow rate and radioactivity, A_c, during a single 5-sec breath (*4,5,18*) were approximated to be constant throughout the inhalation period. The activity in the inlet pipe, $\tilde{A}_i$, was considered to be the activity of the supplied gas, and that in the outlet pipe, $\tilde{A}_o$, was considered the exhaled activity. The activity in gas mask $\tilde{A}_m$ was considered to be the difference between $\tilde{A}_i$ and $\tilde{A}_o$. The S values of these three sources to all TLD positions in Equation 14 were calculated from Equations 1 and 2 with the VADMAP code (*12*). In this calculation, the medium was considered to be air because these sources are outside of the human body. In the simulation, the mask was considered as a rectangular shape of 9 cm × 8 cm × 8 cm, and the inlet and outlet pipes were considered cylinders of 4-mm and 2-cm diameters, respectively.

TABLE 5
Uptake Percentage of $^{15}O_2$, $C^{15}O_2$ and $C^{15}O$ Gases during Inhalation Period

No. of subjects	$^{15}O_2$ (%)	$C^{15}O_2$ (%)	$C^{15}O$ (%)
10	54 ± 8	68 ± 6	72 ± 7

A set of TLDs was placed on each position of the body surface to measure the body surface dose during the successive inhalation of the three gases. Those TLDs were exposed by both the internal transmitted radiation and the background radiation from the mask, inlet and outlet pipes. When the TLD dose at the j-th TLD position during the total inhalation period for these three gases is $D_{t,j}$, the TLD dose at the j-th position for individual gas flow (CO_2, O_2 or CO) can be given by the following equation:

$$D_{g,j}(t) = \frac{fA_g}{A_o} \times D_{t,j}, \quad \text{Eq. 16}$$

where g is a variable for CO_2, O_2 and CO; A_g is the corresponding supplied activity; A_o is the total activity of three gases; fA_g is the absorbed activity of the g-th gas; and f is the percentage uptake. From Equations 14 and 16, the internal dose on the body surface of the j-th TLD due to a single g-th gas supply can be calculated as follows:

$$T_{g,j}(t) = D_{g,j}(t) - D_{g,j}(bg). \quad \text{Eq. 17}$$

As the TLD measurement can be continued during the time course of the clinical PET measurement, the background-subtracted body surface dose from Equation 17 is the only datum during that time. Considering that biological clearance is negligible and only physical decay dominates, the TLD dose due to the residual cumulated activities after the TLD measurement can be estimated using the following equation:

$$T_{g,j}(\infty) = \frac{\int_0^t (1 - e^{-\lambda\tau})\, d\tau + \int_t^\infty (1 - e^{-\lambda t})\, e^{-\lambda(\tau - t)}\, d\tau}{\int_0^t (1 - e^{-\lambda\tau})\, d\tau} T_{g,j}(t), \quad \text{Eq. 18}$$

where t is the time period of the measurement.

Cumulated Activity of Source Organs

T-vectors of 11 TLD positions in Equation 12 were obtained from Equations 17 and 18. The cumulated activities of the 11 source organs, represented by X-vector, were then calculated by using a slightly modified SAND-II unfolding code (*14,15*), based on the successive iteration method. This method starts from the initial guess values X^0, which are given by assuming that the activity concentration is uniform throughout the body. The body surface dose is then calculated from Equation 12, and this value is compared with the measured values of T-vector. The iteration is repeated until the former converges to the latter, within a certain convergence value. This iteration proceeds under the constraint condition that the sum of the cumulated activity of each source organ is equal to the total accumulation of administered activity, such as:

TABLE 6
Body Surface Dose of $^{15}O_2$ and $C^{15}O_2$, Measured by Separate Sets of TLD and a Common Set of TLD (mSv/MBq)

TLD position	O_2 body surface dose measured by separate set of TLD	O_2 body surface dose using common set of TLD	CO_2 body surface dose measured by separate set of TLD	CO_2 body surface dose using common set of TLD
Brain	1.8E-04	4.9E-05	1.3E-04	4.1E-05
Pharynx	1.0E-05	1.2E-05	1.5E-04	1.2E-04
Trachea	9.5E-05	1.1E-04	1.3E-04	1.1E-04
Thyroid	5.4E-05	7.9E-05	1.0E-04	1.2E-04
Heart	9.1E-05	1.0E-04	1.3E-04	1.4E-04
Left lung	7.9E-05	8.8E-05	9.6E-05	1.7E-04
Right lung	7.5E-05	6.4E-05	1.5E-04	1.1E-04
Liver	8.0E-05	5.5E-05	7.7E-05	7.9E-05
Kidney	4.9E-05	4.8E-05	6.7E-05	7.4E-05
Spleen	3.5E-05	1.3E-05	4.7E-05	6.4E-05
Bladder	2.0E-05	1.3E-05	4.0E-05	2.0E-05

$$X_{total} = X_1 + X_2 + X_3 \cdots = \tilde{A}, \qquad \text{Eq. 19}$$

where $\tilde{A}$ is the total uptake given in Equation 13.

Absorbed Dose Calculation

The absorbed doses in 23 target organs were calculated, using Equation 11 with the internal radiation dose estimation system code (*19*), based on the MIRD method (*10*). In this code, two components of the S value are considered, one for penetrating radiation and another for nonpenetrating radiation. The S value of the nonpenetrating radiation for the target organ with wall is approximated to be one for the wall, i.e., the positron energy emitted in that organ is completely absorbed in the wall, and one for other target organs without wall. There is no contribution from source organs to target organs. For penetrating radiation (gamma ray), the S values of 11 source organs to 23 target organs were calculated using Equations 1 and 2, as described above.

The cumulated activities of the other organs included in the remainder of the body can be calculated from their mass fractions to the total because the activity concentration in the remainder of the body was considered to be uniform.

RESULTS

Uptake Measurement of Oxygen-15-Labeled Gases

We have performed an experiment to measure the uptake of inhaled gases on 10 subjects. The experimental arrangement is shown in Figure 2. The $C^{15}O_2$, $^{15}O_2$ and $C^{15}O$ gases produced from the AVF cyclotron at CYRIC were supplied to the controller to manage the flow rate and then to the face gas mask at about 250–350 ml · min^{-1}. The subjects inhaled the gases through the mask under their own control. There were two pipes of polyethylene in the gas mask: a 4-mm-diameter pipe for the inlet gas and a 2-cm-diameter pipe for the outlet gas. To measure the activity of the outlet gas, a NaI(Tl) scintillation detector of 5-cm diameter × 5-cm length and a gas flow meter were placed along the outlet pipe. The NaI(Tl) detector was collimated with the lead of 5 cm × 10-cm cross-section × 20-cm length to shield the background gamma rays from the surroundings. During the PET study, the outlet flow rates due to exhalation and the corresponding activity were measured with these instruments. The inhalation rate of the gas was considered to be equal to the flow rate from the controller. The difference between the radioactivities of the supply gas and outlet gas measured with the NaI(Tl) detector gave the uptake ratio of the inhaled gas. To obtain the activity from the count of the NaI(Tl) detector, a standard source of ^{85}Sr was used for the efficiency calibration because the 511-keV energy of the annihilation photon and the energy of the 514-keV photon emitted from ^{85}Sr are almost the same. The average percentages of uptake for $C^{15}O_2$, $^{15}O_2$ and $C^{15}O$ gases are shown in Table 5 with their s.d. The large s.d. may reflect a wide range in body size of the subjects.

TLD Positions and Body Surface Dose

The body surface dose was measured with TLDs during PET study at CYRIC. The TLDs are BeO. Because the SAF calculation procedure by the VADMAP code (*12*) is independent of energy, the TLD sensitivity to photons for the body surface dose measurement should also be independent of energy. Therefore, we selected the TLD of BeO, whose sensitivity is almost independent of energy.

By the palpation of the medical doctor, the TLDs were placed on the body surface of the subjects at 11 positions close to the

TABLE 7
Cumulated Activities of $^{15}O_2$, $C^{15}O_2$ and $C^{15}O$ for Various Source Organs (kBq · hr/MBq)

Source organ	$^{15}O_2$ (13 yr)	$^{15}O_2$ (Adult)	$C^{15}O_2$ (13 yr)	$C^{15}O_2$ (Adult)	$C^{15}O$ (13 yr)	$C^{15}O$ (Adult)
Major airway (content)	2.15 ± 0.07	1.98 ± 0.52	2.47 ± 0.39	2.14 ± 0.83	2.55 ± 0.22	2.30 ± 0.10
Nasal cavity (content)	1.10 ± 0.15	1.40 ± 0.40	1.65 ± 0.64	1.45 ± 0.31	1.30 ± 0.29	1.61 ± 0.77
Bladder (content)	0.97 ± 0.32	0.69 ± 0.41	1.2 ± 0.35	0.74 ± 0.55	1.30 ± 0.56	0.82 ± 0.31
Kidney	0.51 ± 0.41	0.43 ± 0.25	0.75 ± 0.22	0.53 ± 0.24	0.77 ± 0.24	0.42 ± 0.03
Liver	1.40 ± 0.21	2.20 ± 0.51	1.58 ± 0.10	2.54 ± 0.35	1.68 ± 0.12	3.50 ± 1.29
Lung	4.83 ± 0.21	5.64 ± 1.85	5.80 ± 0.23	5.94 ± 1.21	5.50 ± 0.56	6.22 ± 1.80
Pancreas	0.23 ± 0.06	0.16 ± 0.11	0.20 ± 0.02	0.21 ± 0.11	0.24 ± 0.04	0.13 ± 0.03
Spleen	1.98 ± 0.04	0.29 ± 0.17	0.25 ± 0.05	0.36 ± 0.13	0.27 ± 0.05	0.26 ± 0.03
Heart (cont.)	2.45 ± 0.69	2.90 ± 0.49	2.73 ± 0.38	3.12 ± 0.55	2.67 ± 0.47	3.60 ± 1.00
Brain	1.01 ± 0.36	1.64 ± 0.44	1.46 ± 0.76	2.34 ± 1.44	1.78 ± 0.70	2.90 ± 1.89
Remainder of the body	9.5 ± 1.62	8.21 ± 1.16	14.1 ± 0.98	12.9 ± 1.36	13.48 ± 3.7	11.35 ± 2.2

TABLE 8
Comparison of Cumulated Activities of Various Source Organs, Estimated by this Work and Other Authors due to Continuous Inhalation of $^{15}O_2$, $C^{15}O_2$ and $C^{15}O$ (kBq · hr/MBq)

Source organs	$^{15}O_2$ (Present work)	$^{15}O_2$ (Ref. 4)	$C^{15}O_2$ (Present work)	$C^{15}O_2$ (Ref. 4)	$C^{15}O$ (Present work)	$C^{15}O$ (Ref. 4)	$C^{15}O$ (Ref. 5)
Bladder (content)	0.69		0.74		0.82		0.019
Kidney	0.43	0.24	0.53	0.27	0.42	0.3	0.66
Liver	2.2	1	2.54	1.5	3.5	1.2	2.4
Lung	5.64	6.36*	5.94	1.68*	6.22	5.33*	6.36
Pancreas	0.16		0.21		0.13		0.19
Spleen	0.29	0.42	0.36	0.16	0.26	0.41	1.5
Heart	2.9	1.31	3.12	1.1	3.6	4.83	5.2
Brain	1.64	0.71	2.34	2.9	2.9	5.48	0.29

*Lung including alveolar space and dead space.

following 11 organs: brain, nasal cavity, thyroid, upper respiratory tract, heart, left lung, right lung, liver, kidney, spleen and bladder. The coordinates of the positions for 13-yr-olds and adults were calculated from the MIRD phantom (*11*). In Figure 3, the TLD positions only for 13-yr-old children are shown as Cartesian coordinates together with nearby source organs, although the thyroid is not targeted as a source organ. To measure the body surface dose with TLDs, two different methods were used. First, a separate set of five TLDs was placed at each position on the body surface during inhalation of the individual gas. The mean value of the five TLDs was then considered as the body surface dose at each position for that individual gas. The other method applied a common set of five TLDs at each position for inhalation of $C^{15}O_2$, $^{15}O_2$ and $C^{15}O$. Because the total and individual supplied activities of three gases and their percentages of uptake (from Table 5) are known, the body surface dose due to the individual gas can be calculated as explained above. The first method requires many TLDs and is time-consuming, whereas the second approach is simple and convenient. Sample data of the body surface doses measured by these methods are shown in Table 6.

Cumulated Activities and Absorbed Dose Estimates

Using the body surface dose measured by TLDs and the unfolding technique (*14,15*) from Equation 12, the mean cumulated activities of 11 source organs due to uptake of O_2, CO_2 and CO for two 13-yr-old and five adult subjects are shown in Table 7 together with their s.d. In Table 8, the present results of the cumulated activities for several source organs in adults are compared with the data by Bigler et al. (*4*) and Kearfott (*5*).

The absorbed dose estimates in the 23 target organs due to uptake of O_2, CO_2 and CO were calculated with the MIRD

TABLE 9
Radiation Absorbed Dose Estimates for $^{15}O_2$ (mGy/MBq)

Target organ	Adult (Present work)	Adult Ref. 18	13-yr-old children Present work	13-yr-old children Ref. 18*
Adrenal	2.17E-04	1.7E-04	3.51E-04	2.85E-04
Major airway (wall)	9.98E-03		1.99E-02	
Nasal cavity (wall)	1.34E-02		1.89E-02	
Bladder (wall)	5.98E-04	6.9E-05	1.22E-03	1.06E-04
Stomach (wall)	1.73E-04	9.2E-05	3.04E-04	1.40E-04
SI (wall)	1.35E-04	7.4E-05	2.63E-04	1.21E-04
ULI (wall)	1.38E-04	7.6E-05	2.64E-04	1.20E-04
LLI (wall)	1.21E-04	7.1E-05	2.48E-04	1.12E-04
Kidney	7.93E-04	1.5E-04	1.4E-03	2.40E-04
Liver	8.20E-04	1.3E-04	9.12E-04	2.15E-04
Lung	3.47E-03	2.6E-03	5.11E-03	5.00E-03
Ovary	1.32E-04	6.9E-05	2.6E-04	1.15E-04
Pancreas	1.61E-03	1.1E-04	1.61E-03	1.65E-04
Spleen	9.20E-04	2.6E-04	1.36E-03	4.35E-04
Testes	1.18E-04	6.8E-05	2.43E-04	1.00E-04
Thymus	2.29E-04		3.72E-04	
Thyroid	1.78E-04	1.2E-04	3.22E-04	2.05E-04
Uterus	1.45E-04	6.8E-05	2.89E-04	1.14E-04
Breast	1.68E-04	1.2E-04	2.87E-04	1.65E-04
Brain	6.76E-04		8.06E-04	
Heart (wall)	5.00E-04	3.9E-04	6.45E-04	6.10E-04
Red marrow	6.72E-05	1.0E-04	7.18E-05	1.80E-04
Bone, surface	6.03E-05	8.5E-05	9.50E-05	1.60E-04
EDE (mSv/MBq)	6.6E-04	3.86E-04	1.015E-03	7.2E-04

*Interpolated values between data from 10- and 15-yr-old children.
SI = small intestine; ULI = upper large intestine; LLI = lower large intestine; EDE = effective dose equivalent.

TABLE 10
Radiation Absorbed Dose Estimates for $C^{15}O_2$ (mGy/MBq)

	Adult		13-yr-old children	
Target organ	Present work	Ref. 18	Present work	ICRP 53* (18)
Adrenal	2.57E-04	3.6E-04	4.24E-04	5.4E-04
Major airway (wall)	1.10E-02		2.29E-02	
Nasal cavity (wall)	1.47E-02		2.86E-02	
Bladder (wall)	7.72E-04	3.3E-04	1.55E-03	5.05E-04
Stomach (wall)	2.10E-04	3.2E-04	3.66E-04	5.15E-04
SI (wall)	1.70E-04	3.4E-04	3.22E-04	5.40E-04
ULI (wall)	1.72E-04	3.4E-04	3.22E-04	5.20E-04
LLI (wall)	1.54E-04	3.4E-04	3.02E-04	5.15E-04
Kidney	9.06E-04	3.2E-04	2.03E-03	5.15E-04
Liver	9.92E-04	3.3E-04	1.04E-03	5.25E-04
Lung	3.61E-03	8.7E-04	6.26E-03	1.60E-03
Ovary	1.67E-04	3.2E-04	3.23E-04	5.40E-04
Pancreas	1.81E-03	3.3E-04	1.89E-03	5.50E-04
Spleen	1.20E-03	3.2E-04	1.55E-03	5.25E-04
Testes	1.51E-04	3.3E-04	3.00E-04	4.80E-04
Thymus	2.68E-04		4.44E-04	
Thyroid	2.20E-04	3.0E-04	3.95E-04	5.10E-04
Uterus	1.84E-04	3.2E-04	3.55E-04	5.45E-04
Breast	2.00E-04	3.5E-04	3.45E-04	4.60E-04
Brain	1.05E-03		1.15E-03	
Heart (wall)	5.40E-04		7.29E-04	
Red marrow	0.84E-04	3.1E-04	0.90E-04	5.05E-04
Bone, surface	0.77E-04	3.0E-04	1.18E-04	4.85E-04
EDE (mSv/MBq)	7.33E-04	3.7E-04	1.26E-03	6.1E-04

*Interpolated values between data from 10- and 15-yr-old children.
SI = small intestine; ULI = upper large intestine; LLI = lower large intestine; EDE = effective dose equivalent.

method by using Equation 11 and are shown in Tables 9, 10 and 11, respectively. Our results are compared with the values reported by ICRP (*18*). As the ICRP report does not give the absorbed doses for 13-yr-old subjects, we interpolated those values from the data for 10- and 15-yr-old children.

DISCUSSION

In this gas inhalation study, we estimated the organ biodistribution of ^{15}O-labeled O_2, CO_2 and CO gases from the body surface doses measured with TLDs through the inverse transformation method and, further, the internal absorbed dose estimates were done with the MIRD method, although the number of 13-yr-old subjects are relatively few in the absorbed dose estimation.

Using the uptake percentages of O_2, CO_2 and CO given in Table 5 and Equation 13, we estimated the total uptakes of these gases for continuous inhalation per unit radioactivity, which is ft/λ. These values are around 26, 33 and 35 kBq · hr · MBq^{-1}, respectively. In the calculation of the cumulated activities of the source organs by the SAND-II unfolding code (*14,15*), these values were used as a constraint condition of Equation 19. Bigler et al. (*4*) reported that due to administration of these gases (O_2, CO_2 and CO) for 1 hr at a concentration of 1 mCi per liter of air, the total uptakes are 9.1, 12.3 and 9.7 mCi-hr, respectively. By approximating an inhalation rate of 500 ml of gas for one breath of 5 sec, the total number of breaths for an hour, 720, gives an administration of 360 mCi into the body. The total uptakes of O_2, CO_2 and CO by Bigler et al. (*4*) are then 25, 34 and 27 kBq · hr · MBq^{-1}, respectively. Our results for the total uptakes of O_2 and CO_2 are almost equal to the results reported by Bigler et al. (*4*), but for CO, the difference is 8 kBq · hr · MBq^{-1}. This difference comes from the uptake percentage of CO used by Bigler et al. (*4*), which is around 53%, measured by Bates (*20*). In our study, the uptake percentage of CO is 72% (in Table 5), about 20% higher than that of Bates (*20*).

As described before, we used two methods for obtaining the body surface dose by TLDs: separate TLDs and common TLDs for three different gases. Due to some limitations, we could not compare the doses by these two methods on the same subjects, but a comparison was done on two different subjects of almost the same weights, 72 and 76 kg, respectively. The measured body surface doses in Table 6 show rather good agreement, within about 70% between the methods, except the dose at brain and spleen for O_2, even though the inhalation rate is subject-dependent. The use of separate sets of TLDs for individual gas gives more accurate body surface doses, but the use of a common set of TLDs for all gases is more practically useful to reduce the unnecessary burden.

Table 7 shows the cumulated activities of 11 source organs for O_2, CO_2 and CO gas inhalation averaged for two 13-yr-old and five adult subjects. The highest accumulation organs are the remainder of the body, lung and heart content, in descending order, both for the 13-yr-old and adult subjects. For CO_2 and CO, the next high-accumulation organs in adults are liver, brain and major airway content, whereas for O_2, those organs are the liver, major airway content and brain. In the 13-yr-old subjects, for all three gases, the next highest accumulation organ is the major airway content, and the nasal cavity, liver and brain have almost the same accumulation. For adults, the accumulation of the ^{15}O radioactivities to lung, brain and heart is higher than that for the 13-yr-old subjects, whereas for the major airway it is the reverse.

In the comparative study by Bigler et al. (*4*) for O_2 and CO_2,

TABLE 11
Radiation Absorbed Dose Estimates for $C^{15}O$ (mGy/MBq)

Target organ	Adult		13-yr-old children	
	Present work	Ref. 18	Present work	Ref. 18*
Adrenal	2.48E-04	7.4E-04	4.63E-04	1.19E-03
Major airway (wall)	1.00E-02		2.37E-02	
Nasal cavity (wall)	1.33E-02		2.26E-02	
Bladder (wall)	5.60E-04	2.0E-04	1.65E-03	3.10E-04
Stomach (wall)	1.99E-04	2.4E-04	4.06E-04	3.80E-04
SI (wall)	1.64E-04	2.2E-04	3.64E-04	3.50E-04
ULI (wall)	1.67E-04	2.2E-04	3.63E-04	3.45E-04
LLI (wall)	1.48E-04	2.1E-04	3.44E-04	3.25E-04
Kidney	7.35E-04	6.7E-04	2.10E-03	1.12E-03
Liver	1.00E-03	4.7E-04	1.10E-03	7.70E-04
Lung	2.84E-03	2.3E-03	5.83E-03	4.35E-03
Ovary	1.61E-04	2.0E-04	3.65E-04	3.45E-04
Pancreas	1.32E-03	2.8E-04	2.14E-03	4.35E-04
Spleen	7.22E-04	1.4E-03	1.67E-03	2.25E-03
Testes	1.45E-04	2.0E-04	3.38E-04	2.95E-04
Thymus	2.57E-04		4.76E-04	
Thyroid	2.04E-04	5.1E-04	4.29E-04	8.65E-04
Uterus	1.72E-04	2.0E-04	3.99E-04	3.45E-04
Breast	1.91E-04	2.7E-04	3.76E-04	3.70E-04
Brain	1.10E-03		1.35E-03	
Heart (wall)	5.33E-04	2.1E-03	7.23E-04	3.35E-03
Red marrow	0.88E-04	3.5E-04	1.03E-04	7.05E-04
Bone, surface	0.69E-04	2.7E-04	1.31E-04	5.90E-04
EDE (mSv/MBq)	6.14E-04	5.11E-04	1.21E-03	9.16E-03

*Interpolated values between data from 10- and 15-yr-old children.
SI = small intestine; ULI = upper large intestine; LLI = lower large intestine; EDE = effective dose equivalent.

shown in Table 8, the cumulated activities of kidney, liver and heart in this study, and for lung and spleen of CO_2 inhalation and brain of O_2 inhalation as well, are around 2–3 times higher than those by Bigler et al. (*4*), whereas our results are about 0.7–0.8 times of the results of Bigler et al. for O_2 inhalation (lung and spleen) and CO_2 inhalation (brain). In the model of Bigler et al., for the CO_2 gas, the contribution of the cumulated activity to the lung alveolar gas was lowest among these three gases, which was only 0.27 kBq · hr · MBq^{-1}. As a result, our data of the cumulated activity for the lung were higher than the results of Bigler et al. Because all gases accumulate in the lung immediately after administration, the cumulated activities of the lung should be proportional to the uptake percentage of these gases, which is realized in our experimental results, as shown in Tables 5 and 8.

For CO gas, our data were compared with the results of Bigler et al. (*4*) and Kearfott (*5*). In this comparative study, our data for the cumulated activity of kidney is 0.42 kBq · hr · MBq^{-1}, which is between the values of 0.3 and 0.66 kBq · hr · MBq^{-1} reported by Bigler et al. (*4*) and Kearfott (*5*), respectively. In the case of the brain, a large difference is found between the results of Bigler et al. (*4*) and Kearfott (*5*), whose values were 5.48 and 0.29 kBq · hr · MBq^{-1}, respectively; our result of 2.9 kBq · hr · MBq^{-1} gives an average value of them. The cumulated activity of the liver is 3.5 kBq · hr · MBq^{-1}, which is 3 times higher than the result of Bigler et al. (1.2 kBq · hr · MBq^{-1}), but very close to the reported value of Kearfott (2.4 kBq · hr · MBq^{-1}). The lung cumulated activity of 6.22 kBq · hr · MBq^{-1} shows good agreement with the others' values, and it is especially close to the value of Kearfott. For heart and pancreas, a small difference between the results of Bigler et al. and Kearfott was found. As a whole, a very good agreement between our results and others' results was found, considering the large dispersion of the others' results.

The absorbed doses, reported by ICRP (*18*), for CO_2 and CO are derived from the dose given by Bigler et al. (*4*) and Kearfott (*5*), and the dose for O_2 was derived from the dose reported by Bigler et al. (*4*). A comparison is done in Tables 9–11 between our estimated doses and the ICRP values (*18*). Among the target organs, the nasal cavity and major airway receive highest absorbed doses, and these doses in descending order are CO_2, CO and O_2. For all gases, the critical organs are the nasal cavity and major airway, which includes the pharynx, larynx and trachea. The absorbed dose in the upper airways from the 1-hr inhalation of ^{15}O-labeled CO_2 with 1 mCi/liter of air has been calculated for adult subjects by several authors (*6–9*). In our study, the doses in the nasal cavity and major airway due to inhalation of CO_2 are 1.47×10^{-2} and 1.10×10^{-2} mGy · MBq^{-1}, and the total value is 2.57×10^{-2} mGy · MBq^{-1}. This value is very close to 2.85×10^{-2} mGy · MBq^{-1}, reported by Meyer et al. (*7*), but it is much higher than the results of 2.47×10^{-3} and 8.6×10^{-3} mGy · MBq^{-1} given by Powell et al. (*6*) and Bigler et al. (*9*), respectively. Because the TLD positions of the nasal cavity and major airway are close to the face mask, the doses of these organs have a possibility of overestimation, although we tried to minimize the influence of the background doses from the face mask by simulation.

For all gases, the next highest absorbed dose is in the lung, both for 13-yr-old children and adult subjects. The ICRP doses of lung for O_2 and CO are close to our estimated dose for both 13-yr-old and adult subjects, but for CO_2, our result is about 4 times higher than the dose reported by ICRP. This discrepancy comes from the lower cumulated activity of the lung for the

CO_2 calculated by Bigler et al. (*4*), as seen in Table 8. The brain doses, in descending order, are CO, CO_2 and O_2.

Our result for the heart dose for O_2 is very close to the ICRP value, whereas for CO, our result is about 4 times lower than the ICRP value, both for 13-yr-old and adult subjects, although the cumulated activities of the heart for CO do not show such large discrepancies among the three results given in Table 8.

The doses to pancreas, kidney and spleen in this study are much higher than the ICRP values for all gases, although their cumulated activities, given by three results in Table 8, show a very good agreement. The pancreas is a small organ and lies between liver and spleen; thus, it receives the dose from these two larger organs in addition to its own dose, which contributes to the higher total dose.

The doses of the other target (nonsource) organs were estimated from the cumulated activity of the remainder of the body, considering their mass proportion, and are relatively lower than those of the 10 source organs. The doses of those organs in this study agree with the ICRP reported values within a factor of 2.

Generally speaking, our results show rather good agreement with the ICRP results.

The effective dose equivalent was calculated from the following equation:

$$H_E = \sum_i w_i H_i = \sum_i w_i D_i Q = \sum_i w_i D_i, \quad \text{Eq. 20}$$

where H_i is the dose equivalent of the i-th target organ, D_i is the absorbed dose of i-th target organ and Q is the quality factor (= 1 for beta and gamma rays). We calculated the effective dose equivalent using the weighting factor w_i, given by ICRP (*21*). For comparison, we recalculated the effective dose equivalent given by ICRP (*18*) using the weighting factor given by ICRP (*21*). The extrathoracic airway includes the nasal cavity, pharynx and larynx, and it was considered as a part of the remainder of the body by ICRP (*22*). Although larynx is not included in the nasal cavity in our calculation, we approximated the nasal cavity as the extrathoracic airways and weighting factor of the extrathoracic airways was used to the nasal cavity. The weighting factor of the lung was applied to the average dose of the lung and major airways according to ICRP (*22*). In Tables 9–11, our results of the effective dose equivalent are higher than the ICRP values for all gases because of our higher doses in nasal cavity, major airways, kidney, pancreas and spleen.

CONCLUSION

For continuous inhalation of ^{15}O-labeled gases, we calculated the cumulated activities of 11 source organs based on the TLD method (*13*) and then estimated the internal absorbed doses in 23 target organs by the MIRD method. Our results show generally a good agreement with the values reported by ICRP (*18*), which are based on biological analysis (*4,5*). Among the target organs, the airway is the critical organ, and the absorbed dose is 2.57×10^{-2} mGy · MBq^{-1}, which is very close to 2.85×10^{-2} mGy · MBq^{-1}, reported by Meyer et al. (*7*).

ACKNOWLEDGMENTS

We thank Dr. Takenori Hachiya, Research Institute for Brain and Blood Vessels, Akita, Japan, for providing us the anatomical data on the airways before publication. We also are grateful to Dr. Asif Mustaba Mahmud, Department of Respiratory Medicine, Research Institute of Aging and Cancer, Tohoku University, Japan, for his valuable suggestions regarding the airways.

REFERENCES

1. Russ GA, Bigler RE, Tilbury RS, et al. Whole body scanning and organ imaging with oxygen-15 at the steady state. In: *Proceedings of the 1st World Congress in Nuclear Medicine.* Tokyo: 1974:904–906.
2. Jones T, Chesler DA, Ter-Pogossian MM. The continuous inhalation of oxygen-15 for regional oxygen extraction in the brain of man. *Br J Radiol* 1976;49:339–343.
3. Subramanyan R, Alpert NM, Hoop BJ, Brownell GL, Tavera JM. A model for regional cerebral oxygen distribution during continuous inhalation of $^{15}O_2$, $C^{15}O_2$ and $C^{15}O$. *J Nucl Med* 1978;19:48–53.
4. Bigler RE, Sgouros G. Biological analysis and dosimetry for 15O-labeled $^{15}O_2$, $C^{15}O_2$ and $C^{15}O$ gases administered continuously by inhalation. *J Nucl Med* 1983;24:431–437.
5. Kearfott KJ. Absorbed dose estimates for positron emission tomography (PET): $C^{15}O$, ^{11}CO and $CO^{15}O$. *J Nucl Med* 1982;23:1031–1037.
6. Powell GF, Schuchard RA, Reff CS, et al. Radiation absorbed dose to major airway mucosa from inhaled oxygen-15 leveled carbon dioxide. *Ann Neurol* 1984;(suppl 15):S107–S109.
7. Meyer E, Yamamoto LY, Evans AC, Tyler JL, Dicsic M, Feindel W. Radiation dose to upper airways from inhaled oxygen-15 carbon dioxide. *J Nucl Med* 1987;28:234–239.
8. Powell GF, Schuchard RA, Reff CS, et al. Beta particle dose to the major airway from inhaled gas [Abstract]. *J Nucl Med* 1984;25:P39.
9. Bigler RE, Sgouros G, Zanzonico PB, et al. Radiation dose to the respiratory airway linings from inhalation of (^{15}O)-carbon dioxide [Abstract]. *J Nucl Med* 1985;26:P39.
10. Loevinger R, Buidinger TF, Watson EE, eds. *MIRD primer for absorbed dose calculations.* New York: Society of Nuclear Medicine, Inc.; 1991:1–17.
11. Cristy M, Eckerman KF. *Specific absorbed fractions of energy at various ages from internal photon sources. 1. Methods.* Oak Ridge, TN: Oak Ridge National Laboratory; 1987:3–83.
12. Yamaguchi Y, Togawa O, Honma T. The VADMAP code to calculate the SAF of photon-code description and the performance. Tokyo: Japan Atomic Energy Research Institute, JAERI M87-186; 1987:1–42.
13. Matsumoto M, Nakamura T, Watabe H, Itoh M, Hatazawa J. Estimation of organ biodistribution and absorbed dose from experimental measurement with TLDs in PET studies. *Med Biol Eng Comput* 1993;31:151–156.
14. McElroy WN, Berg S, Crockett T, Hawkins RG. A computer automated iterative method for neutron flux spectra determination by foil activation. Air Force Weapons Laboratory, AFWL-TR-67-41; 1967.
15. Oster CA, McElroy WN, Simons RL, Lippincott EP, Odette GR. A modified Monte-Carlo program for SAND-II with solution weighting and error analysis. Hanford Engineering Development Laboratory, HEDL-TME 76-60, UC-79b; 1976.
16. Synder WS, Ford MA, Warner GG, Fisfer HL Jr. Estimation of absorbed fractions for monoenergetic photon sources uniformly distributed in various organs of a heterogeneous phantom. *MIRD pamphlet no. 5.* New York: Society of Nuclear Medicine 1969;10:3–43.
17. Harima Y, Sakamoto Y, Tanaka S, Kawai M. Validity of geometric-progression formula in approximating gamma ray buildup factors. *Nucl Sci Eng* 1986;94:24–35.
18. Annals of the ICRP, vol. 18, nos. 1–4. *ICRP Publication 53.* Oxford: Pergamon Press; 1987:65–71.
19. Hongo S, Takeshita H, Yamaguchi H. A computer program: IDES (Internal Radiation Dose Estimation System). In: *Present status of internal radiation dose estimation code development.* Tokyo: Japan Health Physics Society; 1992:17–27.
20. Bates DV. The uptake of carbon monoxide in health and in emphysema. *Clin Sci* 1952;11:21–32.
21. Annals of the ICRP, vol. 21, nos. 1–3. *ICRP Publication 60.* Oxford: Pergamon; 1991:1–9.
22. Annals of the ICRP, vol. 24, no. 4. *ICRP Publication 68.* Oxford: Pergamon; 1994:1–19.